Research Article Vol. 29, No. 6 / 15 March 2021 / Optics Express 8685
Optics EXPRESS

All-polymer whispering gallery mode resonators for gas sensing

CÉDRIC LEMIEUX-LEDUC, RÉGIS GUERTIN, MARC-ANTOINE BIANKI, AND YVES-ALAIN PETER*

Department of Engineering Physics, Polytechnique Montréal, P.O. Box 6079, Station Centre-Ville, Montréal, QC H3C 3A7, Canada
*yves-alain.peter@polymtl.ca

Abstract: Sensitivity of polymeric microdisks is evaluated for selected compounds in their vapor phase such as humidity, isopropanol, toluene, limonene, 1-butanol, and pentanoic acid (valeric acid). Among these compounds, pentanoic acid exhibits the highest sensitivity (23 pm/ppm) with a limit of detection estimated to be around 0.6 ppm. We are interested in the contribution of the geometry deformation due to polymer swelling on the sensitivity as it may be engineered to improve performance of gas sensing devices. Experimental observations show a trend where sensitivity to humidity increased with the ratio of the undercut over the radius of the microcavity.

1. Introduction

Gas sensors are widely used today in numerous applications such as air quality monitoring [1] and disease detection [2]. They have since been developed on thermal [3], electrochemical [4], mechanical [5] and optical detection principles [6]. Even though electrochemical gas sensors received a lot of attention during the past decades, optical gas sensors are seen as an attractive alternative as they are compatible with hostile environments because of their immunity to electromagnetic noise and their ability to be used in explosive media [7]. Diverse optical gas sensors thus far have been developed based on numerous principles such as mid-infrared absorption [8], photonic crystals [9], fiber Bragg gratings [10], Fabry-Perot interferometers [11] and whispering gallery mode resonators [12].

Whispering gallery mode (WGM) resonators are a type of optical cavity that has been widely investigated for gas sensing as well as for the detection of nanoparticles, proteins, and bacteria [13,14]. In these resonators, light is confined in a round-shaped cavity by total internal reflection, forcing it to follow the circumference of the structure. They are well-known for their high quality factor (Q) and small modal volume. Resonance occurs after a full round trip of the cavity for wavelengths λ_m (resonant modes) that satisfy the following interference condition:

$$m\lambda_m = 2\pi R n_{\text{eff}}, \tag{1}$$

where m is a positive integer associated to the mode number, R is the radius of the cavity, and n_{eff} the effective refractive index of the mode. WGM resonators can be found in several geometries such as microrings, microdisks, microtoroids, and microspheres [15]. A shift in the frequency of the resonant modes can be observed when the optical path is modified, which could indicate a change in the circumference of the resonator, a change in the refractive index, or both. Several sensors use polymers as an absorbing medium in order to enhance the modification of these properties to improve performance in the detection of gases [11]. The use of a polymeric coating helps functionalize high-Q microcavities like silica microtoroids [16] or integrated microcavities like microrings [17,18] to achieve enhanced sensing performance.

Another emerging strategy is fabricating polymeric resonators to maximize the interaction of light with the absorbing medium [19,20]. Fabrication of polymeric structures is possible

#417703 https://doi.org/10.1364/OE.417703
Journal © 2021 Received 11 Jan 2021; revised 15 Feb 2021; accepted 21 Feb 2021; published 5 Mar 2021

Optics EXPRESS

using SU-8, which is an epoxy-based polymer that can be selectively cross-linked with UV light. SU-8 absorption to humidity [21] and other compounds [22] has been investigated, revealing possibilities to use it in gas sensing applications. Integrated SU-8 microdisks coupled to a waveguide were fabricated for humidity sensing, requiring only a single photolithography step on a SiO_2/Si substrate by Eryürek *et al.* [23]. Though performance of SU-8 in humidity detection has been presented, its sensitivity to other volatile compounds has not been thoroughly probed in the context of gas sensing. Furthermore, it is also expected that sensitivity to volatile compounds can be enhanced in an all-polymer WGM microresonator standing on a pillar, facilitating polymer swelling.

In this work, sensitivity of SU-8 WGM microdisk resonators attached to a silicon pillar is assessed for several volatile compounds to evaluate its usage in gas sensing applications with compact photonic systems. Herein, we suppose that the partial release of the attachment of the polymer to the substrate can significantly improve the WGM sensitivity in gas detection since its deformation is less restricted. To determine if the partial detachment of the polymeric microdisks can improve sensitivity, humidity sensitivity of these microresonators is evaluated by probing microdisks with different radii and undercut lengths. Other properties such as response time and temperature sensitivity are examined.

2. Methods

2.1. Sensing mechanism

The gas sensing mechanism used for optical microresonators is based on tracking resonant wavelength variations of the optical cavity and correlating these variations to quantities of analyte absorbed by the sensing medium. Upon gas absorption, the spectral shift $\Delta\lambda$ of the resonant wavelengths can be generally described by the following relation:

$$\frac{\Delta\lambda}{\lambda} = \frac{\Delta R}{R} + \frac{\Delta n}{n}. \tag{2}$$

In Eq. (2), there are two mechanisms contributing to the spectral shift caused by the absorption of a gas into the polymer: the change in radius ΔR due to polymer swelling and the change in refractive index Δn caused by the insertion of the analyte and the formation of a polymer-analyte blend. Both mechanisms can be linked to the analyte concentration absorbed by the polymer. The partition coefficient K_{p-a} is the ratio of the concentration of an analyte between two media, which are the polymer (c_p) and air (c_a) in our case:

$$K_{p-a} = \frac{c_p}{c_a}. \tag{3}$$

The volume fraction of analyte within the polymer ϕ_a is related to the volume expansion from polymer swelling and is proportional to the concentration of analyte within the polymer [11]:

$$\phi_a \propto c_p = K_{p-a} c_a. \tag{4}$$

The polymer swelling term ($\frac{\Delta R}{R}$) in Eq. (2) is often neglected since its contribution is usually small compared to a variation of refractive index, which is the case for glassy polymers like polymethyl methacrylate (PMMA). However, this mechanism can contribute equally or more than variations of the refractive index for given polymers as it has been observed by St-Gelais *et al.* while assessing the sensitivity to m-xylene of in-plane Fabry-Perot resonators functionalized with polydimethylsiloxane (PDMS) [11]. Therefore, investigating highly-absorbing polymers may turn out to be advantageous to improve performance of optical devices for gas sensing applications [24].

Optics EXPRESS

2.2. Fabrication

Herein, SU-8 is used in this study because of its excellent optical and mechanical properties. In microelectronics, it is mainly used as a negative photoresist for photolithography. SU-8 has also been used in the development of several applications from microelectromechanical systems [25] to biosensing devices [26]. Since it can easily be cured by UV light, a photomask with disk patterns can be used to directly form cross-linked SU-8 microdisks on a silicon substrate. This method has also been used to fabricate high-Q PMMA microdisk resonators [27]. Sensitivity of in-plane Fabry-Perot resonators functionalized with SU-8 to several volatile organic compounds (VOCs) has been previously assessed [28]. Based on observations made by Schmid *et al.* on the hygroscopic properties of SU-8 using all-polymer mechanical resonators [21], it is expected that polymer swelling has a non-negligible influence on the sensitivity of SU-8 devices with volatile compounds in general.

The refractive index of SU-8 is relatively close to glass (n = 1.58 at 1550 nm) with high transparency in the infrared (IR) in the conventional telecommunications bands (1260 – 1675 nm), making it desirable in numerous applications in optics. To fabricate the microdisk resonators, SU-8 (SU-8 2000.5, MicroChem) is spin-coated on a 4-inch Si wafer (<100>, type P, Resistivity 0-100 Ω) to obtain a thickness of ~ 700 nm and is selectively cured by UV light to form disks using a photomask. The silicon substrate is then isotropically etched with SF_6 by reactive-ion etching (RIE) to form the pillars supporting the disks (Plasmalab 100, Oxford Instruments). Figure 1 shows SEM images of a SU-8 microdisk with a 50-µm radius and a 10-µm undercut.

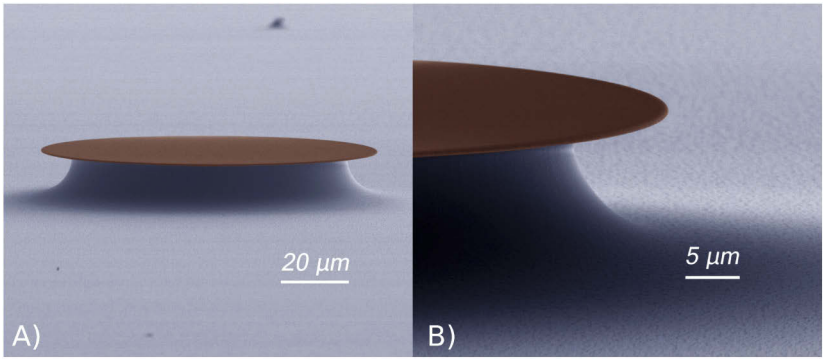

Fig. 1. SEM images of a SU-8 WGM microcavity (radius = 50 µm and undercut = 10 µm).

2.3. Experimental setup

The experimental setup illustrated in Fig. 2 allows fast readout of the transmission spectrum from a WGM microcavity while being exposed to an analyte concentration. The optical transmission measurement of the cavity is performed using a tunable IR laser source (TLS) (Agilent 8164B) connected to a 1-µm tapered fiber optically coupled to the cavity. The sample is held on a 5-axis stage and the tapered fiber on a second one to adjust coupling between the tapered fiber and the microcavity. A fiber polarization controller (FPC) is used to maximize the extinction ratio of the optical signal. The output signal is measured with an optical powermeter (Keysight N7744A) as the wavelength of the tunable laser sweeps over a desired range to form a spectrum. Spectra are acquired with a range of 20 nm (between 1500 nm and 1600 nm) with 24500 data points and an average acquisition time of ~ 1 s per spectrum.

The generation of analyte vapors is enabled by injecting nitrogen inside a bubbler containing the analyte in its liquid phase. A communication interface (Model 400, CCR Process Products) sets the different flows of nitrogen by controlling flow meters (Mass-Flo Controller, MKS

Optics EXPRESS

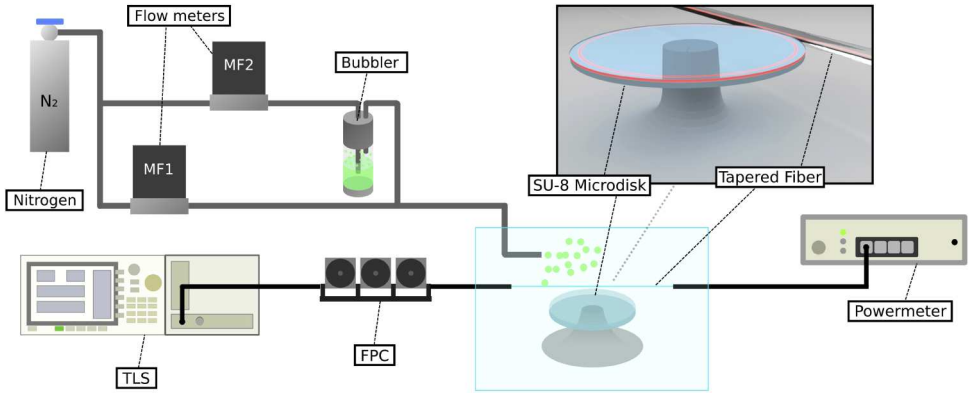

Fig. 2. Experimental setup used to determine sensitivity to a gas.

Instruments). One is used as the carrier gas with a high nitrogen flow (MF1, between 280 and 350 sccm) while the other is injected into the bubbler to bring the liquid compound to its vapor phase using a much lower nitrogen flow (MF2, between 1 and 20 sccm). The analyte in its vapor phase is then combined to the carrier gas to dilute it in nitrogen while the blend is brought to the sample. Different analyte concentrations are accessible by tuning the nitrogen flows.

To extract the sensitivity of the cavity to the investigated analyte, the resonant peak position is recorded as the cavity is exposed to different concentrations of analyte following a desired pattern of steps. Between each step, the sample is purged with nitrogen to define a baseline for the recorded spectral shift. This allows the evaluation of the spectral shifts of the cavity for all tested concentrations. Error on the shift values is estimated to be around 3 pm and is mainly attributed to environmental variations and repeatability of laser wavelength tuning to a given position. Figure 3 shows a resonant peak being red-shifted as it is exposed to different humidity concentrations.

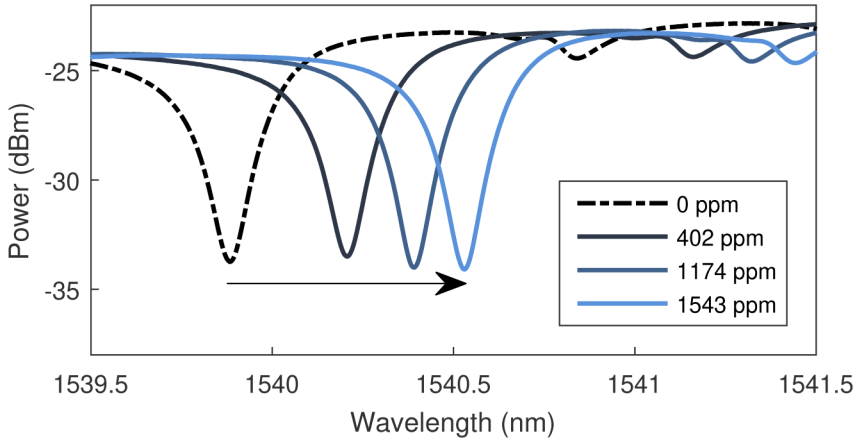

Fig. 3. A WGM resonant peak being shifted as the cavity is being exposed to humidity concentrations of 402 ppm, 1174 ppm, and 1543 ppm.

Optics EXPRESS

Sensitivity S is then extracted by computing the slope of the spectral shift $\Delta\lambda$ in function of the analyte concentration Δc evaluated using a resonant mode located at λ:

$$S = \frac{\Delta\lambda}{\Delta c}. \tag{5}$$

A thermocouple probe is used to measure the air temperature surrounding the sample. Observations are achieved at 23 °C and slow variations of about 1 °C can be observed over several hours of measurements. This variation in temperature can cause spectral shifts larger than 100 pm, which can often be much larger than the shifts caused by analyte absorption. While these fluctuations may lead to discrepancies in the measurements, this thermally-induced shift can be corrected during post-processing of the data. Here, the regression of a spline function is applied on the data points from the baseline and is then subtracted from the raw data. For a cavity with a 50 µm radius ($R = R_{disk}$) and a 10 µm undercut ($u = R_{disk} - R_{pillar}$), a quality factor Q ($Q = \lambda/\delta\lambda$ where $\delta\lambda$ is the FWHM of the resonant peak) of about 1.47×10^4 is obtained for a resonant peak located at 1540 nm. The free spectral range (FSR) for the same cavity is around 5 nm and is consistent with the approximation $FSR \approx \lambda^2/2\pi nR \approx 5.01$ nm (using $n_{eff} \approx n = 1.58$).

3. Results and discussion

3.1. Sensitivity to volatile organic compounds

Sensitivity of the SU-8 microdisk ($R = 50$ µm, $u = 10$ µm) is first measured for humidity and a value of 0.39 pm/ppm is obtained. Figure 4 shows the spectral shift of a resonant peak versus humidity concentration. A linear regression is applied to extract the sensitivity. The coefficient of determination R^2 of this regression is 0.994, indicating a good agreement between the data and the linear fit. The error bars are smaller than the square markers (from 3 to 5 pm).

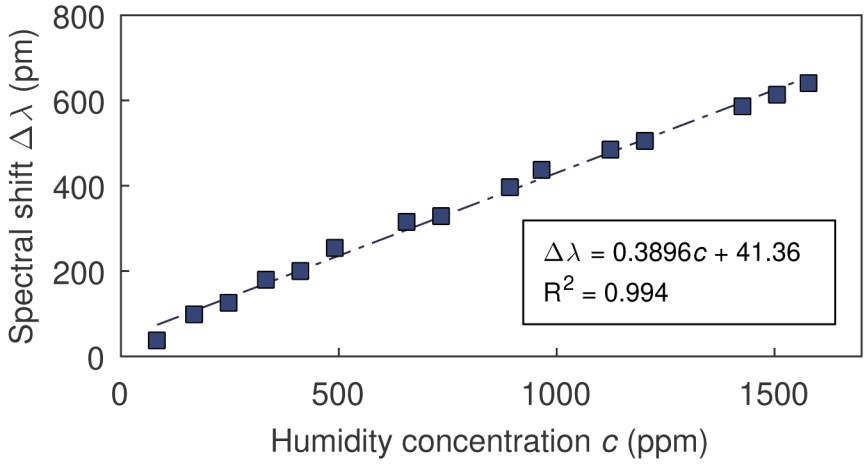

Fig. 4. Spectral shift of a WGM resonant peak versus humidity concentration.

Sensitivity to isopropanol, toluene, limonene, 1-butanol, and pentanoic acid is also assessed using this methodology and also responded linearly. Measured sensitivities and limits of detection (LOD) for several analytes are reported in Table 1 with the wavelength of the resonant mode and the range of tested concentrations at which the sensitivity is measured. The highest sensitivity measured is 23 pm/ppm with pentanoic acid. The error on sensitivity originates from the confidence interval (2σ) of the determination of the linear fit (Curve Fitting Toolbox, MATLAB). The limit of detection for a given compound is calculated by taking three times the standard noise of the measurement (3σ) and dividing it by the sensitivity S (LOD = $3\sigma/S$).

Optics EXPRESS

Table 1. Measured sensitivities, limits of detection, and probed range of concentrations with a SU-8 microdisk (R = 50 µm, u = 10 µm). The concentration range is limited by the characterization setup.

Compound	Wavelength (nm)	Sensitivity (pm/ppm)	LOD (ppm)	Concentration range (ppm)
Humidity	1540	0.39 ± 0.02	11	0 - 1577
Isopropanol	1569	0.07 ± 0.01	64	0 - 3530
Toluene	1581	0.34 ± 0.04	32	0 - 781
Limonene	1591	2.3 ± 0.4	6	0 - 133
1-Butanol	1504	0.10 ± 0.01	26	0 - 482
Pentanoic acid	1576	23 ± 1	0.6	0 - 23

With the results from Table 1, we observe that SU-8 is sensitive to several compounds with sensitivities located on different orders of magnitude. Humidity, toluene, and 1-butanol are approximately on the same order of magnitude (0.10 – 0.39 pm/ppm). By testing even more compounds, we may observe a broad range of sensitivities. Using SU-8 as a single sensing material in a gas sensing system may exhibit signal contamination from its cross sensitivity in presence of multiple analytes. It may however serve useful in a multiplexed sensor architecture where contributions coming from the detection of multiple analytes at the same time can be decoupled by an array of nonspecific sensors [24]. Table 2 reports LODs for the same tested compounds using different methods and are compared with the obtained values in this work.

Table 2. Comparison of the computed LODs with values reported in other works using different methods. Some values of LOD are compared to gas chromatography-mass spectroscopy (GCMS) as no sensor detecting these compounds has been found in literature.

Compound	LOD - This work (ppm)	LOD - Reference (ppm)	Method - Reference
Humidity	11	0.17	Mechanical resonator [29]
Isopropanol	64	20	SnO_2 nanorods [30]
Toluene	32	1.2	Mechanical resonator [31]
Limonene	6	0.0017	GCMS [32]
1-Butanol	26	72	Quartz crystal microbalance [33]
Pentanoic acid	0.6	0.00014	GCMS [34]

To further investigate these results, the sensitivity for these VOCs is plotted in function of the saturated vapor pressure in Fig. 5. The relationship between the sensitivity and the saturation vapor pressure can be associated to a change in the partition coefficient K_{p-a} between the gas and the polymer. The partition coefficient highly depends on the polymer and the vapor properties, and the affinity between them. This affinity can be expressed by multiple parameters such as solubility parameters which represent the degree of interaction between two given compounds. Models for K_{p-a} suggest that the partition coefficient is inversely proportional to the saturated vapor pressure [35].

In Fig. 5, a trend is observed where compounds with a low saturated vapor pressure tend to have a high sensitivity than those with a high saturated vapor pressure. The linear trend on the logarithmic scale indicates that sensitivity is then inversely proportional to the saturated vapor pressure of the analyte, which suggests that sensitivity is proportional to the partition coefficient. This relationship is observed in other studies involving analyte absorption by a polymer for VOC detection like in the case of Scholten *et al.* using an optofluidic ring resonator coated with PDMS [36]. Values of the partition coefficient for SU-8 have so far not yet been reported in the literature for any compound. Such information could help further investigate gas sensitivity of SU-8 with other analytes. SU-8 has a strong affinity with polar solvents and interaction with

Optics EXPRESS

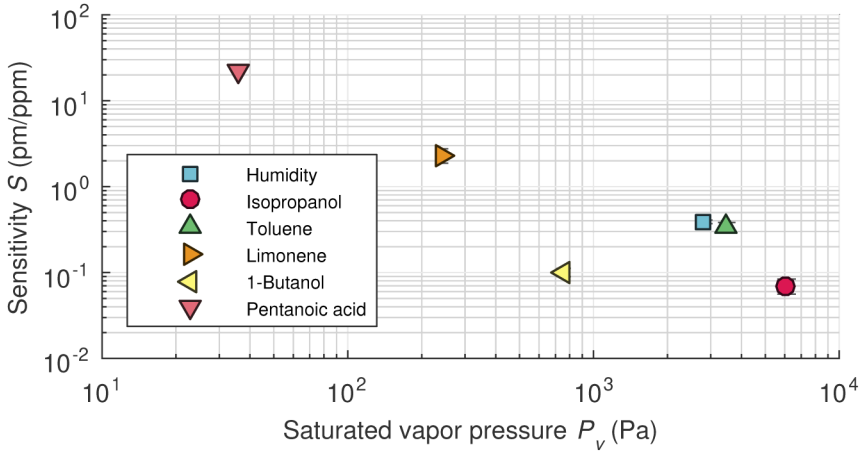

Fig. 5. Sensitivity of the studied gases plotted with respect to their saturated vapor pressure at 23 °C.

some compounds may ultimately lead to dissolution of the polymer as it can be observed with acetone and methanol [22].

3.2. *Impact of geometry deformation on sensitivity*

The contribution of the polymeric swelling mechanism to sensitivity in Eq. (2) is related to the extent of attachment of the disk to the pillar supporting it. For instance, a disk fully attached to the substrate should essentially have no polymer swelling contributing to sensitivity since its displacement is restricted by the attachment between SU-8 and the substrate. In the opposite case, a disk without any support will deform freely upon gas absorption. The disk would then have the largest contribution possible from polymer swelling to sensitivity since the deformation is not restricted. With the hypothesis that the radius deformation ΔR is proportional to the undercut u ($\Delta R \approx u \cdot \Delta\epsilon$ with ϵ being the relative strain along the radial axis due to polymer swelling) and using Eq. (2) and (5), the following relationship is obtained:

$$S = \lambda \left(\frac{\Delta\epsilon}{\Delta c} \frac{u}{R} + \frac{1}{n} \frac{\Delta n}{\Delta c} \right), \tag{6}$$

where $\frac{\Delta\epsilon}{\Delta c}$ and $\frac{\Delta n}{\Delta c}$ are the expansion and optical coefficients, respectively. Considering that ΔR is proportional to u, then $\frac{\Delta\epsilon}{\Delta c}$ is proportional to the ratio u/R. Therefore, the sensitivity S increases as the size of the pillar decreases (the undercut u increases). This model is illustrated in Fig. 6. A uniform distribution of the analyte within the disk is assumed so that the deformation of the disk is homogeneous in all directions ($\epsilon_x = \epsilon_y = \epsilon_z$). Axisymmetric deformation of a polymeric disk attached to a pillar is modeled through finite element modeling (COMSOL) by substituting the thermal expansion coefficient with the expansion coefficient to humidity from Schmid *et al.* [21]. A linear expansion of 0.01% is applied for different values of u and R and the variation of the radius at equilibrium ΔR is calculated. The results show good agreement with the hypothesis that the radius variation ΔR scales linearly with the undercut u for values of R between 50 and 100 µm. Figure 7 illustrates these results where the radial expansion of the disk increases by the same magnitude with the undercut for any values of R until approximately $u \approx 25$ µm before slightly diverging. It is interesting to note that ΔR is not equal to $(0.01\%)u$ and that there seems to be an additional factor with a value of approximately 1.3. This factor slightly changes by modifying values of the Young's modulus E and the Poisson ratio ν, but can be rounded to ~ 1.3 (with E = 4 GPa and $\nu = 0.22$).

Optics EXPRESS

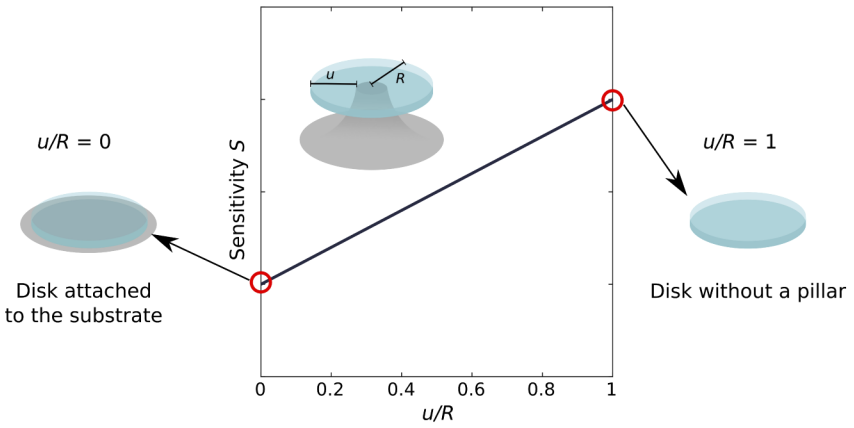

Fig. 6. Illustration of the expected effect of u/R ratio on the sensitivity of the cavity (assuming $\frac{\Delta\epsilon}{\Delta c}>0$).

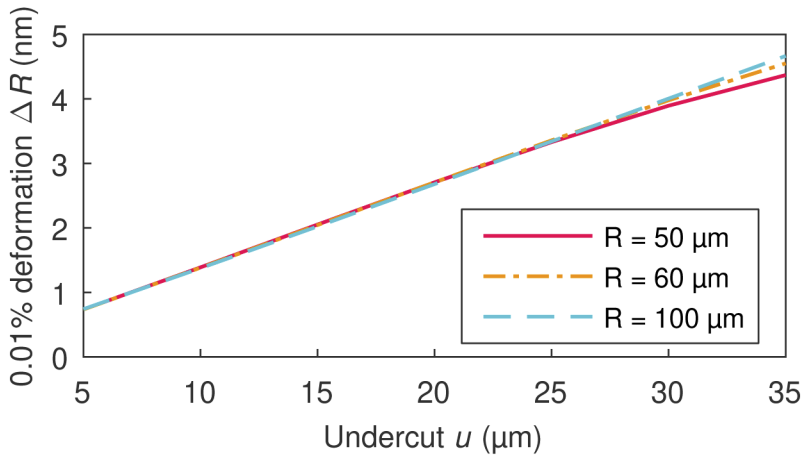

Fig. 7. Results of the expansion simulations using finite element modeling for disks with radii of 50 μm, 60 μm, and 100 μm. Results are obtained using an axisymmetric mechanical model of a disk on a pillar.

Optics EXPRESS

Sensitivity is thus expected to increase as the ratio of the undercut over the disk radius is increased. To verify this experimentally, different ratios are obtained by fabricating microdisks with different radii and undercuts. Sensitivity to humidity is then measured for these samples. Results are shown in Fig. 8 supporting that sensitivity is proportional to the u/R ratio. The error on the ratio u/R is determined by assuming a maximal variation of 1 µm on both the variation of the radius due to optical lithography and the obtained undercut from the SF_6 plasma etching. In order to further validate the model, Eq. (6) can be fitted to extract its coefficients $\frac{\Delta\epsilon}{\Delta c}$ and $\frac{\Delta n}{\Delta c}$ by normalizing the sensitivities S at the probed wavelength λ. The R^2 value of the obtained regression is 0.845, implying slight variations of the data with the linear fit. Extracted values for $\frac{\Delta\epsilon}{\Delta c}$ and $\frac{\Delta n}{\Delta c}$ are comparable to other reported constants as shown in Table 3 (using 1%RH = 277.9 ppm).

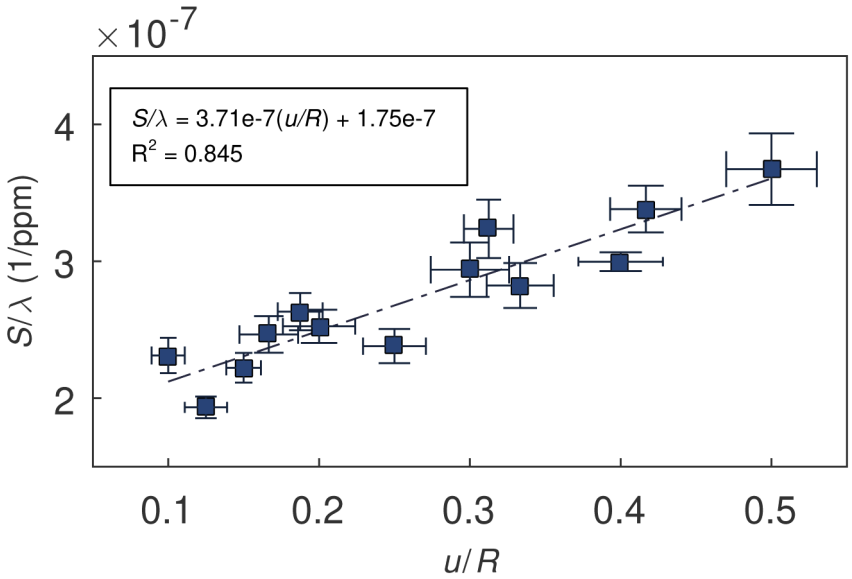

Fig. 8. Humidity sensitivity compared to the u/R ratio.

Table 3. Comparison of extracted coefficients for $\frac{\Delta\epsilon}{\Delta c}$ and $\frac{\Delta n}{\Delta c}$ with literature for humidity (converted from ppm to %RH). Coefficients for $\frac{\Delta\epsilon}{\Delta c}$ from [21] are converted from volume to linear expansion coefficients by dividing them by 3.

Coefficient	This work	Literature
$\frac{\Delta\epsilon}{\Delta c}$ (10^{-5} 1/%RH)	7.9	0.8-1.7 [21]
$\frac{\Delta n}{\Delta c}$ (10^{-5} RIU/%RH)	7	7.7 [23]

In Table 3, we note that the extracted value $\frac{\Delta\epsilon}{\Delta c}$ is large (~ 7.9) compared to hygroscopic coefficients obtained by Schmid *et al.* [21]. It is possible that the difference in the fabrication steps can have a large impact on the final properties of the polymer, which is also witnessed in their work as they computed and compared this coefficient for different mechanical structures. The value of $\frac{\Delta n}{\Delta c}$ is compared with the estimated value of sensitivity obtained by Eryürek *et al.* with SU-8 microdisks integrated with waveguides on silicon dioxide [23]. The authors evaluated the expansion of the disk and estimated that there is essentially no polymer swelling contributing to the sensitivity mechanism for that configuration and that it is mainly a variation of the microresonator refractive index. This experiment can be repeated with a different polymer

Optics EXPRESS

and a different analyte to further investigate the potential of the model depicted in Eq. (6). It could be used to accurately extract these coefficients related to the gas sensing properties of a polymer and it may potentially be used to predict the sensitivity of a given optical gas sensing device through modeling.

3.3. Response time

We evaluate the response time of SU-8 microdisks upon exposure to humidity concentrations. In Fig. 9, a concentration of 1784 ppm humidity is applied for each step (light blue zones) before getting purged by pure nitrogen. All the four steps reach a similar spectral shift while exposed to the same humidity concentration after purging with nitrogen, indicating a good repeatability of the absorption/desorption process. The time to reach approximately 90% of the maximal shift value is 100 s on average whilst it drops to around 14 s to reach 75%. Two mechanisms seem to be contributing to the shift: one where the resonant peak rapidly shifts within the first few seconds and a second one that is characterized by a slow drift of the spectral shift. Response time is evaluated by fitting a sum of two exponential functions with the following model:

$$\Delta\lambda = A_1\left(1 - B_1 e^{\frac{t-t_0}{\tau_1}}\right) + A_2\left(1 - B_2 e^{\frac{t-t_0}{\tau_2}}\right), \tag{7}$$

to consider the two mechanisms where A_1, A_2, B_1 and B_2 are fitting parameters, t_0 the initial time where the concentration is applied and τ_1 and τ_2 the computed response time of both mechanisms. By fitting Eq. (7) on the third step shown in Fig. 9, values of 3 s and 78 s are obtained for τ_1 and τ_2, showing the contribution of the fast and slow mechanisms.

The response is relatively fast compared to electrochemical sensors where their response time can often exceed minutes. The fast drift can be associated to the diffusion of the analyte through the thin SU-8 disk and the slow drift to the required amount of time for the analyte concentration to reach an equilibrium in the setup and near the microresonator.

3.4. Temperature sensitivity

Temperature sensitivity has to be considered for applications involving environmental monitoring since sensors may be exposed to large temperature fluctuations. SU-8 is estimated to have a thermal linear expansion coefficient of approximately 5.2×10^{-5} 1/K [37] and a thermo-optic coefficient of about -1.8×10^{-4} RIU/K [38]. Therefore, small variations in temperature are expected to generate significant spectral shifts, which can contaminate the signal coming from analyte absorption. Temperature sensitivity is measured by controlling the temperature of the sample with a Peltier cooler and adjusting it with a feedback control system. A sensitivity to temperature of −169.7 pm/°C is measured (R = 60 µm and u = 10 µm) with a R^2 of 0.993. Figure 10 illustrates the spectral shifts observed at different temperatures for a resonant peak near 1568 nm.

The temperature sensitivity is significant compared to the sensitivity values in Table 1 and should not be neglected when designing a gas sensor using SU-8. Interestingly, Eq. (6) can be used to calculate a value of sensitivity using the previously presented thermal expansion and thermo-optic coefficients instead of $\frac{\Delta\epsilon}{\Delta c}$ and $\frac{\Delta n}{\Delta c}$. Using a u/R ratio of 1/6 and n = 1.58 at λ = 1568 nm, we calculate a sensitivity of approximately −161.5 pm/°C, which is within 5% from the measured value. While it has been used to extract coefficients related to gas sensing properties, this model may also work for other measurands.

Optics EXPRESS

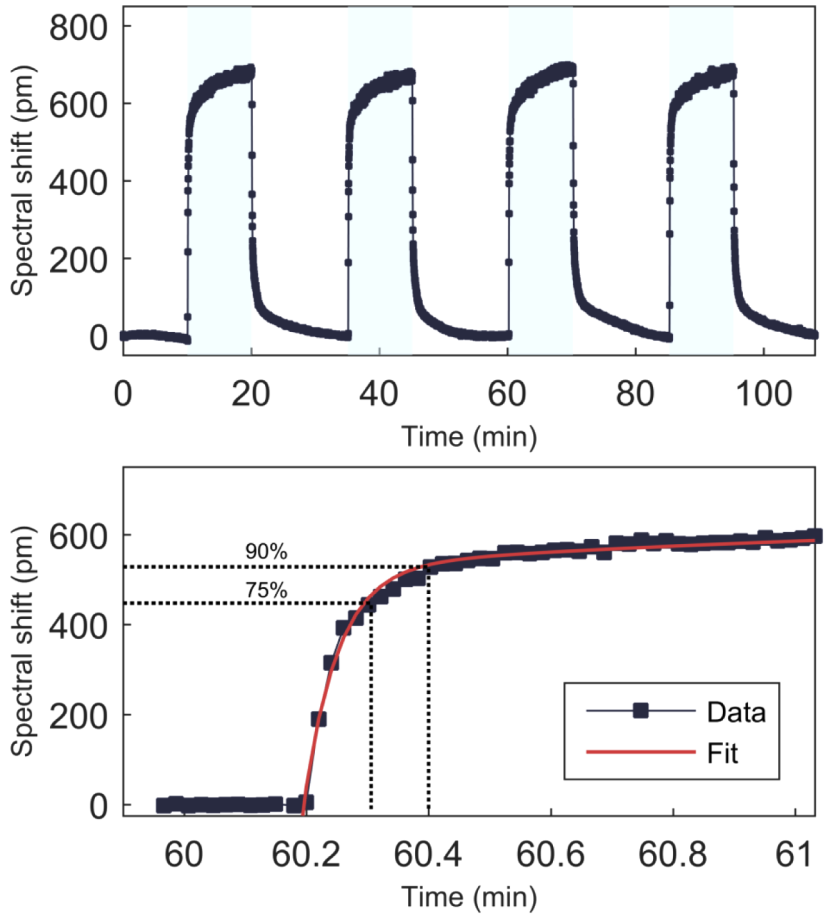

Fig. 9. Top: response time of the cavity (R = 50 µm and u = 10 µm). A concentration of 1784 ppm is applied at each step. Bottom: magnification of the transient regime where the resonant peak shifts rapidly within a few seconds then slowly drifts.

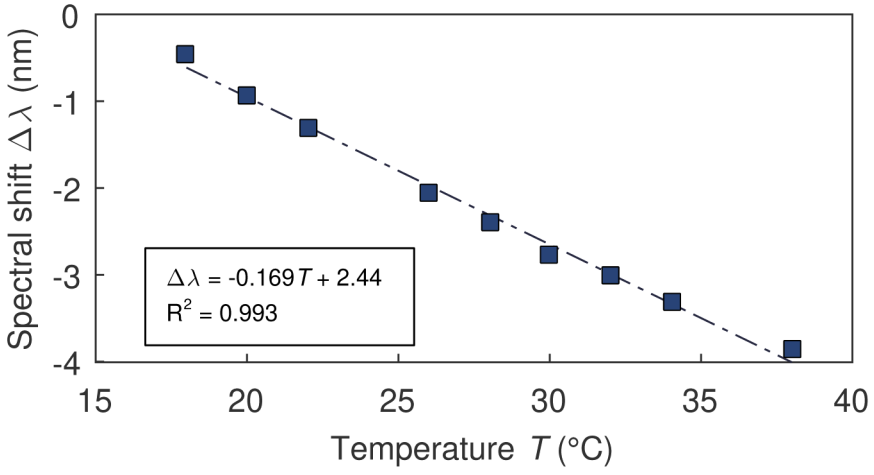

Fig. 10. Temperature sensitivity of a SU-8 microdisk measured from 18 to 38 °C.

Optics EXPRESS

4. Conclusion

Microdisks made from SU-8 are fabricated and their sensitivity to several volatile organic compounds such as humidity, isopropanol, toluene, limonene, 1-butanol, and pentanoic acid is assessed. For all these compounds, the structure exhibited a linear response. SU-8 has the highest sensitivity for pentanoic acid with 23 pm/ppm. For a disk standing on a pillar, we observed that its sensitivity to humidity could be improved with increased undercut size, thus reducing the diameter of the pillar and the attachment to the disk. This is explained by the polymer swelling mechanism, which is less restricted since the size of the pillar supporting the disk decreases in size. Thus, it allows the optical path of the WGM microcavity to be modified to a greater extent upon analyte absorption by the polymer. A model has been developed to investigate the swelling behaviour of SU-8, which has the potential to be used in studying gas sensing properties of polymers with different analytes. Characterization also included evaluation of the response time and the temperature sensitivity. Even though SU-8 is sensitive to several analytes, it is very promising for integrated photonic systems for gas sensing that rely on a configuration of nonspecific sensors.

Funding. Fonds de recherche du Québec – Nature et technologies (208540); Natural Sciences and Engineering Research Council of Canada (RGPIN-2020-06692, CGS M).

Disclosures. The authors declare no conflicts of interest.

References

1. M. I. Mead, O. Popoola, G. Stewart, P. Landshoff, M. Calleja, M. Hayes, J. Baldovi, M. McLeod, T. Hodgson, J. Dicks, A. Lewis, J. Cohen, R. Baron, J. Saffell, and R. Jones, "The use of electrochemical sensors for monitoring urban air quality in low-cost, high-density networks," Atmos. Environ. **70**, 186–203 (2013).
2. A. P. Turner and N. Magan, "Electronic noses and disease diagnostics," Nat. Rev. Microbiol. **2**(2), 161–166 (2004).
3. N.-H. Park, T. Akamatsu, T. Itoh, N. Izu, and W. Shin, "Calorimetric thermoelectric gas sensor for the detection of hydrogen, methane and mixed gases," Sensors **14**(5), 8350–8362 (2014).
4. Y.-F. Sun, S.-B. Liu, F.-L. Meng, J.-Y. Liu, Z. Jin, L.-T. Kong, and J.-H. Liu, "Metal oxide nanostructures and their gas sensing properties: a review," Sensors **12**(3), 2610–2631 (2012).
5. M. Benetti, D. Cannatà, E. Verona, A. P. Papavlu, V. C. Dinca, T. Lippert, M. Dinescu, and F. Di Pietrantonio, "Highly selective surface acoustic wave e-nose implemented by laser direct writing," Sens. Actuators, B **283**, 154–162 (2019).
6. J. Hodgkinson and R. P. Tatam, "Optical gas sensing: a review," Meas. Sci. Technol. **24**(1), 012004 (2013).
7. A. Tripathy, S. Pramanik, J. Cho, J. Santhosh, and N. Abu Osman, "Role of morphological structure, doping, and coating of different materials in the sensing characteristics of humidity sensors," Sensors **14**(9), 16343–16422 (2014).
8. C. Ranacher, C. Consani, A. Tortschanoff, R. Jannesari, M. Bergmeister, T. Grille, and B. Jakoby, "Mid-infrared absorption gas sensing using a silicon strip waveguide," Sens. Actuators, A **277**, 117–123 (2018).
9. Y. Chang, D. Hasan, B. Dong, J. Wei, Y. Ma, G. Zhou, K. W. Ang, and C. Lee, "All-dielectric surface-enhanced infrared absorption-based gas sensor using guided resonance," ACS Appl. Mater. Interfaces **10**(44), 38272–38279 (2018).
10. S. Sridevi, K. Vasu, N. Bhat, S. Asokan, and A. Sood, "Ultra sensitive NO2 gas detection using the reduced graphene oxide coated etched fiber Bragg gratings," Sens. Actuators, B **223**, 481–486 (2016).
11. R. St-Gelais, G. Mackey, J. Saunders, J. Zhou, A. Leblanc-Hotte, A. Poulin, J. A. Barnes, H.-P. Loock, R. S. Brown, and Y.-A. Peter, "Gas sensing using polymer-functionalized deformable Fabry–Perot interferometers," Sens. Actuators, B **182**, 45–52 (2013).
12. J. T. Robinson, L. Chen, and M. Lipson, "On-chip gas detection in silicon optical microcavities," Opt. Express **16**(6), 4296–4301 (2008).
13. M. R. Foreman, J. D. Swaim, and F. Vollmer, "Whispering gallery mode sensors," Adv. Opt. Photonics **7**(2), 168–240 (2015).
14. H. Ghali, H. Chibli, J. Nadeau, P. Bianucci, and Y.-A. Peter, "Real-time detection of staphylococcus aureus using whispering gallery mode optical microdisks," Biosensors **6**(2), 20 (2016).
15. K. J. Vahala, "Optical microcavities," Nature **424**(6950), 839–846 (2003).
16. S. Mehrabani, P. Kwong, M. Gupta, and A. M. Armani, "Hybrid microcavity humidity sensor," Appl. Phys. Lett. **102**(24), 241101 (2013).
17. G. Mi, C. Horvath, and V. Van, "Silicon photonic dual-gas sensor for H2 and CO2 detection," Opt. Express **25**(14), 16250–16259 (2017).
18. D. Fu, J. Chung, Q. Liu, R. Raziq, J. S. Kee, M. K. Park, S. Valiyaveettil, and P. Lee, "Polymer coated silicon microring device for the detection of sub-ppm volatile organic compounds," Sens. Actuators, B **257**, 136–142 (2018).
19. M.-K. Bae, J. A. Lim, S. Kim, and Y.-W. Song, "Ultra-highly sensitive optical gas sensors based on chemomechanical polymer-incorporated fiber interferometer," Opt. Express **21**(2), 2018–2023 (2013).

Optics EXPRESS

20. L. Labrador-Páez, K. Soler-Carracedo, M. Hernández-Rodríguez, I. R. Martín, T. Carmon, and L. L. Martin, "Liquid whispering-gallery-mode resonator as a humidity sensor," Opt. Express **25**(2), 1165–1172 (2017).
21. S. Schmid, S. Kühne, and C. Hierold, "Influence of air humidity on polymeric microresonators," J. Micromech. Microeng. **19**(6), 065018 (2009).
22. J. E. Saunders, H. Chen, C. Brauer, M. Clayton, W. Chen, J. A. Barnes, and H.-P. Loock, "Quantitative diffusion and swelling kinetic measurements using large-angle interferometric refractometry," Soft Matter **11**(45), 8746–8757 (2015).
23. M. Eryürek, Z. Tasdemir, Y. Karadag, S. Anand, N. Kılınç, B. Alaca, and A. Kiraz, "Integrated humidity sensor based on SU-8 polymer microdisk microresonator," Sens. Actuators, B **242**, 1115–1120 (2017).
24. K. J. Albert, N. S. Lewis, C. L. Schauer, G. A. Sotzing, S. E. Stitzel, T. P. Vaid, and D. R. Walt, "Cross-reactive chemical sensor arrays," Chem. Rev. **100**(7), 2595–2626 (2000).
25. P. Abgrall, V. Conedera, H. Camon, A.-M. Gue, and N.-T. Nguyen, "SU-8 as a structural material for labs-on-chips and microelectromechanical systems," Electrophoresis **28**(24), 4539–4551 (2007).
26. Y. Wang, J.-H. Pai, H.-H. Lai, C. E. Sims, M. Bachman, G. Li, and N. L. Allbritton, "Surface graft polymerization of SU-8 for bio-MEMS applications," J. Micromech. Microeng. **17**(7), 1371–1380 (2007).
27. T. Grossmann, M. Hauser, T. Beck, C. Gohn-Kreuz, M. Karl, H. Kalt, C. Vannahme, and T. Mappes, "High-Q conical polymeric microcavities," Appl. Phys. Lett. **96**(1), 013303 (2010).
28. P. Jubinville, R. Guertin, L. Erbilgin, W. Skene, and Y.-A. Peter, "Selective in-plane fabry-pérot gas sensor functionalized with polymer," in *2017 International Conference on Optical MEMS and Nanophotonics*, (IEEE, 2017), pp. 1–2.
29. D. Southworth, L. Bellan, Y. Linzon, H. G. Craighead, and J. Parpia, "Stress-based vapor sensing using resonant microbridges," Appl. Phys. Lett. **96**(16), 163503 (2010).
30. D. Hu, B. Han, R. Han, S. Deng, Y. Wang, Q. Li, and Y. Wang, "Sno2 nanorods based sensing material as an isopropanol vapor sensor," New J. Chem. **38**(6), 2443–2450 (2014).
31. S. B. Truax, K. S. Demirci, L. A. Beardslee, Y. Luzinova, A. Hierlemann, B. Mizaikoff, and O. Brand, "Mass-sensitive detection of gas-phase volatile organics using disk microresonators," Anal. Chem. **83**(9), 3305–3311 (2011).
32. X.-B. Xu, K. Murtada, and J. Pawliszyn, "Determination of selected volatile terpenes in fish samples via solid phase microextraction arrow coupled with gc-ms," Talanta **221**, 121446 (2021).
33. X. Fan and B. Du, "Selective detection of trace 1-butanol by QCM sensor coated with copolymer P (HEMA-co-MA)," Sens. Actuators, B **160**(1), 724–729 (2011).
34. Z. Tang and Y. Duan, "Fabrication of porous ionic liquid polymer as solid-phase microextraction coating for analysis of organic acids by gas chromatography–mass spectrometry," Talanta **172**, 45–52 (2017).
35. S. J. Patrash and E. T. Zellers, "Characterization of polymeric surface acoustic wave sensor coatings and semiempirical models of sensor responses to organic vapors," Anal. Chem. **65**(15), 2055–2066 (1993).
36. K. Scholten, X. Fan, and E. T. Zellers, "A microfabricated optofluidic ring resonator for sensitive, high-speed detection of volatile organic compounds," Lab Chip **14**(19), 3873–3880 (2014).
37. H. Lorenz, M. Laudon, and P. Renaud, "Mechanical characterization of a new high-aspect-ratio near UV-photoresist," Microelectron. Eng. **41-42**, 371–374 (1998).
38. Y.-F. Liu, X.-B. Wang, J. Sun, H.-J. Gu, X.-Q. Sun, C.-M. Chen, F. Wang, and D.-M. Zhang, "Thermal field analysis of polymer/silica hybrid waveguide thermo-optic switch," Opt. Commun. **356**, 79–83 (2015).